A Comprehensive Study on Nanoparticle–Surfactant Solutions for Foam-assisted Enhanced Oil Recovery: In-Depth Understanding via High Pressure Micromodel Visualization Experiments

Jinesh Machale[1], *Farzan Sahari* Moghaddam[1], *Maziyar* Mahmoodi[1], *Ali* Telmadarreie[2], *Lesley Anne* James[1*]

[1] Department of Process Engineering, Faculty of Engineering and Applied Science, Memorial University of Newfoundland, St. John's, NL A1C 5S7, Canada.
[2] Cnergreen Corporation, Life Sciences Innovation Hub (LSIH) 3655 36 St NW, Calgary, AB T2L 1Y8, Canada.

Abstract. Foam-assisted enhanced oil recovery has gathered substantial interest within scientific and industrial sectors due to its versatile functionalities. These involve its effectiveness as a mobility controller, penetrating un-swept zones, increasing the viscosity at the injection front, redirecting fluid flow from high to low permeability zones, and reducing the interfacial tension between immiscible phases. Foam formation and stability remain challenging tasks influenced by various factors, including pressure gradients across the media, petrophysical properties, interactions between chemical additives in foam and oil, velocities of gaseous and aqueous phases, concentration of surfactant in aqueous phase, salts, and temperature. Conventionally, foam performance has been evaluated via incremental oil recovery and pressure drop across a core. This approach cannot visually observe foam formation. Due to the thermodynamic instability of foams, fluctuations in pressure differentials are observed, requiring a significant duration for stabilization. Consequently, direct visualization techniques in micromodels provide an effective means to comprehend pore-scale phenomena. This approach enhances our understanding of foam behavior within porous media. The present study employs a visualization pressure cell with a micromodel to evaluate the performance of a novel customized nanoparticle–surfactant solution for foam-assisted enhanced oil recovery. An *ex-situ* foam was formed utilizing nanoparticle–surfactant solution and nitrogen gas within the porous media. A systematic experimental methodology was employed to visualize the process of foam migration and their behavior within porous media. Moreover, the impact of pressure, salinity, and the heterogeneity of the porous media on foam performance are considered in the present study. A noteworthy increase of 13.7–26.6% in oil production was observed in a series of foam flooding experiments in micromodels. Additionally, the assessment of foam in diverting residual oil from high to low permeability zones was noticed.

1 Introduction

Considering the heavy reliance on fossil fuels and the fact that renewable energy sources are not yet able to meet increasing energy demands, developing more effective oil recovery techniques is vital. Usual primary and secondary oil recovery techniques typically recover merely 10–40% of the crude oil from a reservoir. Most of the oil remains trapped due to the significant interfacial tension between fluid phases, robust capillary forces, and prevailing electrostatic interactions between the rock formations and the crude oil [1,2]. Tertiary oil recovery, commonly referred to as enhanced oil recovery (EOR), established techniques involve the injection of steam, various gases (such as methane, carbon dioxide, and nitrogen), numerous chemical additives (such as polymer, alkali, surfactant, and nanoparticles) to increase oil recover [3–5]. The primary objective of EOR methods is to improve the mobility of trapped oil [1], which can be accomplished by either increasing the viscosity of aqueous phase or reducing the viscosity of crude oil. Techniques such as steam and gas injection are particularly effective in decreasing oil viscosity. In contrast, chemical injection strategies can reduce the IFT between immiscible fluids, increase the viscosity of the aqueous phase, and alter the wettability of rock (often oil-wet to moderate water-wet or oil-wet to strong water-wet) to aid additional oil recovery.

These techniques retain several challenges, including constraints related to the fingering and channeling of gas within porous media, premature gas breakthrough, insufficient stability of chemical additives

* Corresponding author: ljames@mun.ca

under high reservoir temperatures, limited penetration of gases and chemical additives into low-permeability rock zones, and the loss of chemical additives due to adsorption onto rock surfaces [5–8]. These challenges reduce the efficacy and effectiveness of EOR techniques, thereby impacting their performance. Numerous studies signified that the challenges mentioned above can be effectively mitigated by applying foam-assisted EOR [9–11]. This method represents a distinctive approach wherein the foam facilitates mobility control and reduces the IFT between immiscible fluids [11].

Foam is essentially a dispersion of a gaseous phase in a continuous liquid phase. Additionally, a gas–liquid interface separates a thin liquid film from a gas phase. Typically, foam structure includes three elementary parts: lamella, Plateau border, and node [12,13]. In porous media, flowing foam typically exhibits three distinct phases: continuous gaseous phase, immobile bubble phase, and mobile foam phase [14]. Both bubble dimensions and pressure differences across the porous media govern the movement of the gaseous phase. Accordingly, it exhibits continuous mobility and transitions to immobility within the porous medium. On the other hand, the aqueous phase penetrates the granular structure of the substrate, occupying the pores. In porous media, foam formation normally happens through three main mechanisms: snap-off, leave-behind, and lamella or bubble division [14,15]. Characteristically, foam generated within porous media is classified into two primary types: strong and weak foams. A prominent increase in pressure difference characterizes strong foam formations, whereas weak foams demonstrate a comparatively reasonable increase in pressure difference across the porous media [16].

Effective employment of foam-assisted EOR relies on the foam stability in the reservoir-like condition. Various properties significantly influence foam stability, including the rate at which foam is generated and the pressure difference across the porous media [14]. Several chemical additives, essentially surfactants along with nanoparticles, polymer, and alkali, demonstrated effective agents in stabilizing the foam in the porous media. Readers are encouraged to go through the review articles on role of chemical additives in effective foam-assisted EOR applications [17–19].

In our prior study, we methodically analyzed the efficacy of foam-assisted EOR implementation. In addition, we have outlined a comprehensive workflow for conducting several experiments and factors affecting the foam quality, stability, and performance in oil recovery applications. We have also provided several perspectives on integrating experimental measurements with reservoir simulation, explaining the impact of individual foam parameters. Readers are encouraged to refer to the article for more insight [20]. In the present study, we expanded upon previous investigations [20,21] and conducted a series of flooding experiments within micromodels to evaluate the effectiveness of a customized-nanoparticle–surfactant foam for enhancing oil recovery. A methodical experimental approach was employed to observe the dynamics of foam migration and its interaction within pore space of the micromodel. Furthermore, we compared the performance of the customized nanoparticle–surfactant with that of a commercial alpha-olefin sulfonate, both in single and dual permeability micromodels.

2 Materials and methodology

2.1 Materials

In the present study, a customized nanoparticle–surfactant solution provided by Cnergreen Corp. (Canada) was used. In addition, we compared the provided nanoparticle–surfactant solution with commercial alpha-olefin sulfonate surfactant from Stepan (USA). Hibernia light crude oil with a density of 878 kg m^{-3}, viscosity of 2.5 mPa s, API gravity of 35, and asphaltene content below 1% was utilized. A synthetic brine with a concentration of 35,000 mg L^{-1} was prepared. The salts were procured from Fisher Scientific (Canada) with assay ≥ 99.0%. The details regarding the composition of the salts used are outlined in Table 1.

Table 1. Components of the synthetic brine.

Salt	NaCl	$CaCl_2$	$MgCl_2$	KCl	Na_2SO_4
Concentration (g L^{-1})	29.53	4.31	0.90	0.14	0.11

2.2 Methodology

2.2.1 Micromodel flooding experiments

The micromodel flooding experiments were conducted in the Visualization Pressure Cell (VPC) developed at the Hibernia Research Laboratory at the Memorial University of Newfoundland. The setup photograph and detailed schematic is shown in Figure 1 (a,b). A series of experiments were carried out at 30°C and 17,237 kPa in a single and dual-permeability micromodels (see Figure 1c). The single permeability micromodel exhibits a porosity of 19.36 ± 0.42. In contrast, the dual permeability micromodel demonstrates a porosity of 15.37 ± 0.13 in the low permeability zone and 8.00 ± 0.08 in the high permeability zone. The initial step involved placing the cleaned micromodel within the high-pressure cell and subsequently sealing the top by connecting the vessel cap. An overburden pressure of 24131 kPa was then applied by injecting silicon oil. The micromodel was first saturated with synthetic brine followed by crude oil, with approximately 2–3 pore volumes (PV) of each fluid. Further, gas flooding commenced initially to mobilize saturated oil by injecting nitrogen gas, followed by foam injection, and again by gas flooding. The foam was generated *ex-situ* by passing nitrogen gas and surfactant solution through a sapphire visual cell before injecting it into the micromodel. The injection flow rate for the experimental fluids was maintained at 2 PV per day. Figure 1d illustrates the end of each fluid flooding in a single permeability micromodel.

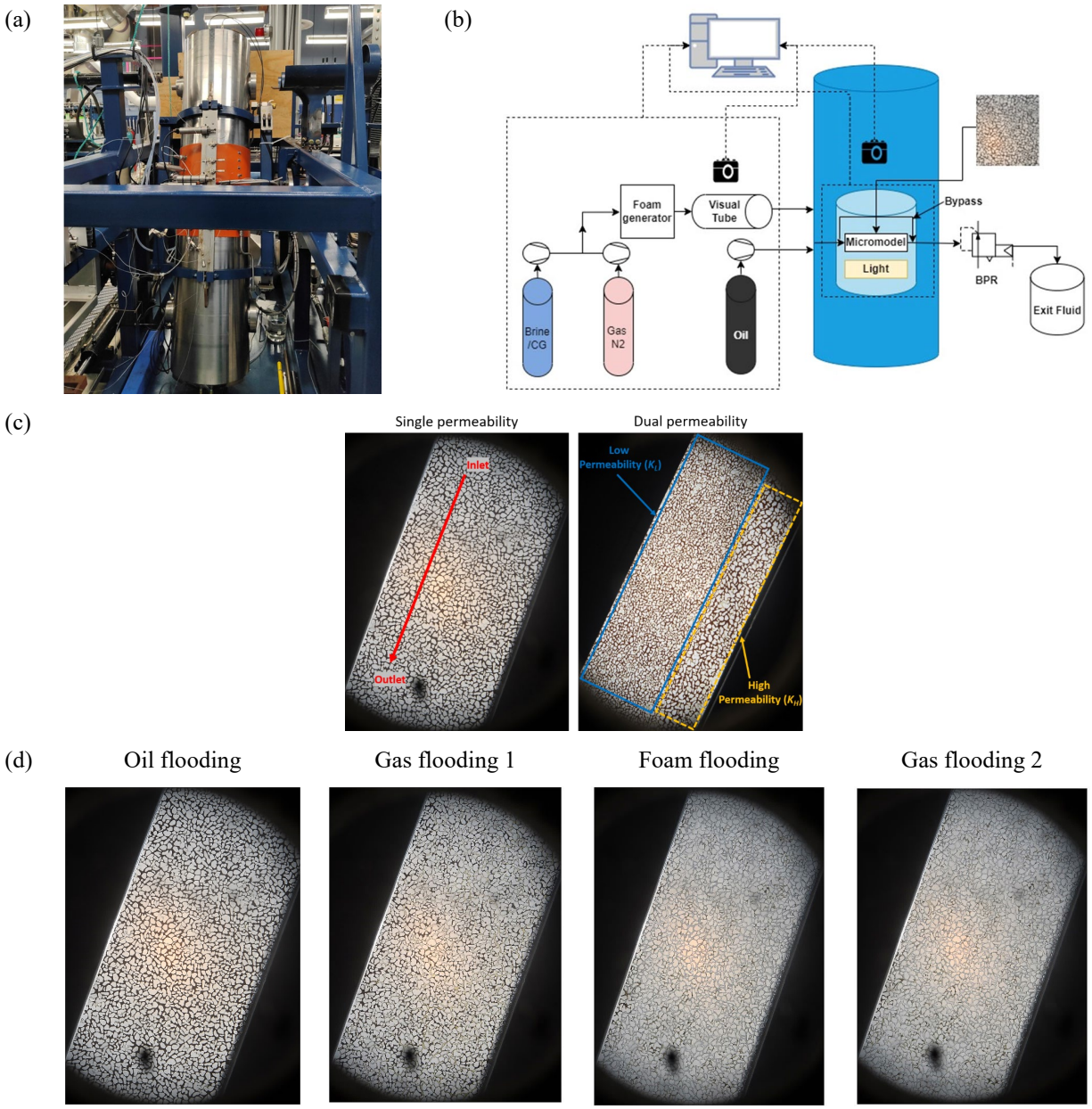

Fig. 1. (a) Photograph and (b) schematic of the experimental setup, (c) single (left) and dual permeability (right) micromodels used in the present study, (d) photographs of single permeability micromodel at the end of each fluid flooding.

2.2.2 Micromodel visualization and image processing

A high-resolution camera [model: EOR 6D, make: Canon (Japan)] equipped with 105 mm macro lens was utilized in capturing displacement of fluids in the micromodel. An image processing algorithm was developed using the IMAQ vision module of LabVIEW, which was optimized to interpret the visual data captured during the displacement of multiphase fluid (i.e., crude oil, gas, and foam) in a micromodel. The algorithm includes six steps, implemented in order: initialization, monochrome plane extraction, non-uniform background correction, segmentation, particle analysis, and calculation [22]. Visual interpretations were conducted based on differences in color and shape. Furthermore, regions of interest (ROI) were outlined for both single and dual permeability micromodels using the captured images. The high permeability ROI is denoted as K_H, while the low permeability ROI is denoted as K_L. Readers are encouraged to refer to our previous study for further details on the image processing algorithm executed in the present study [22].

3 Results and discussion

Figure 2 (a, b) shows the total oil recovery using gas–foam flooding in a single permeability micromodel. Initially, nitrogen gas flooding was carried out, which recovered ~22–28% of oil. Figure 2c illustrates the displacement of initial oil by nitrogen gas, demonstrating its efficacy in

mobilizing and pushing the oil towards the production outlet. Moreover, the increase in ΔP indicates the initial mobilization of the oil phase. This could be due to the resistance encountered by the gas displacing the oil through the pores. As the gas displaces the oil and moves through the pore network, the resistance diminishes, resulting in a decrease in ΔP. However, instances of viscous fingering were observed within micromodels, which can be attributable to the comparatively lower viscosity and density of nitrogen gas than crude oil [23–25].

Further, the utilization of foam generated via alpha-olefin sulfonate and customized-nanoparticle–surfactant samples resulted in the recovery of an additional 49.2% and 37.7% of oil, respectively. The correlation between pressure difference variation and the increase in oil recovery corresponding to injected foam is illustrated in Figures 2 (a,b). Typically, primary mechanisms of residual oil mobilization during foam injection are conventionally attributed to direct displacement and oil emulsification [26]. As discussed in the introduction section, the phenomenon of foam generation typically occurs within the porous media via three principal methods: snap-off or pinch-off, leave-behind, and lamellae division. The methods mentioned above were identified in both instances of foam generation employing alpha-olefin sulfonate and a customized nanoparticle-surfactant system. Their respective illustration is shown in Figure 2(d,e). However, lamellae division governed throughout the foam flow within the single permeability micromodel.

Although higher oil recovery was achieved in the case of the alpha-olefin sulfonate sample (see Table 2), several irregularities were observed in the ΔP values (see Figure 2a). These findings suggest that despite the effective generation and dissemination of foam utilizing alpha-olefin sulfonate, the foam exhibits instability and vulnerability to rupture. This phenomenon can be attributed to the migration of surfactant molecules towards the edges of foam film, leading to the shrinking of foam lamellae thickness and eventual rupture [12]. On the contrary, foam generated via customized-nanoparticle–surfactant demonstrated a notable stability increase compared with alpha-olefin sulfonate-generated foam. Variations in the ΔP were noted with customized-nanoparticle–surfactant-generated foam, albeit generally maintaining levels around 200 kPa during foam injection (See Figure 2b). This phenomenon can be attributed to incorporating customized nanoparticles within the foam structure. Nanoparticles present at the gas-liquid interface of foam not only abets in developing a robust and consistent foam film but also accumulate within the foam lamella, forming an interfacial shield that boosts film viscoelasticity, ultimately slowing film thinning and coalescence [27,28].

At the second gas injection step, minor changes in the oil recovery and a drop in the pressure difference were observed post alpha-olefin sulfonate-generated foam (see Figure 2a). However, in the case of customized-nanoparticle–surfactant-generated foam, a sharp increase in oil production was observed, followed by a plateau in the oil production during second gas injection. Concurrently, the pressure differential exhibited a similar pattern (see Figure 2b). This phenomenon aligns with percolation theory, wherein fluid tends to flow through the most permeable (or larger) pores, continuing as desirable pathways unless diverted [29]. Upon injection of customized-nanoparticle–surfactant-induced foam, it flows into the larger pores. As the foam collapsed, it created a network of nanoparticles within the porous media. During the second gas injection, the gas primarily moved through the smaller pores that were it initially encounters the resistance to flow due to the nanoparticles network. This caused a sudden rise in the ΔP between 6.5 and 7 PV, leading to an increase in oil production (see Figure 2b). As the nanoparticle network shifts, the gas encounters less resistance and the flow becomes steady. At this point, a noteworthy drop in the ΔP was observed, and the oil recovery curve reached plateau.

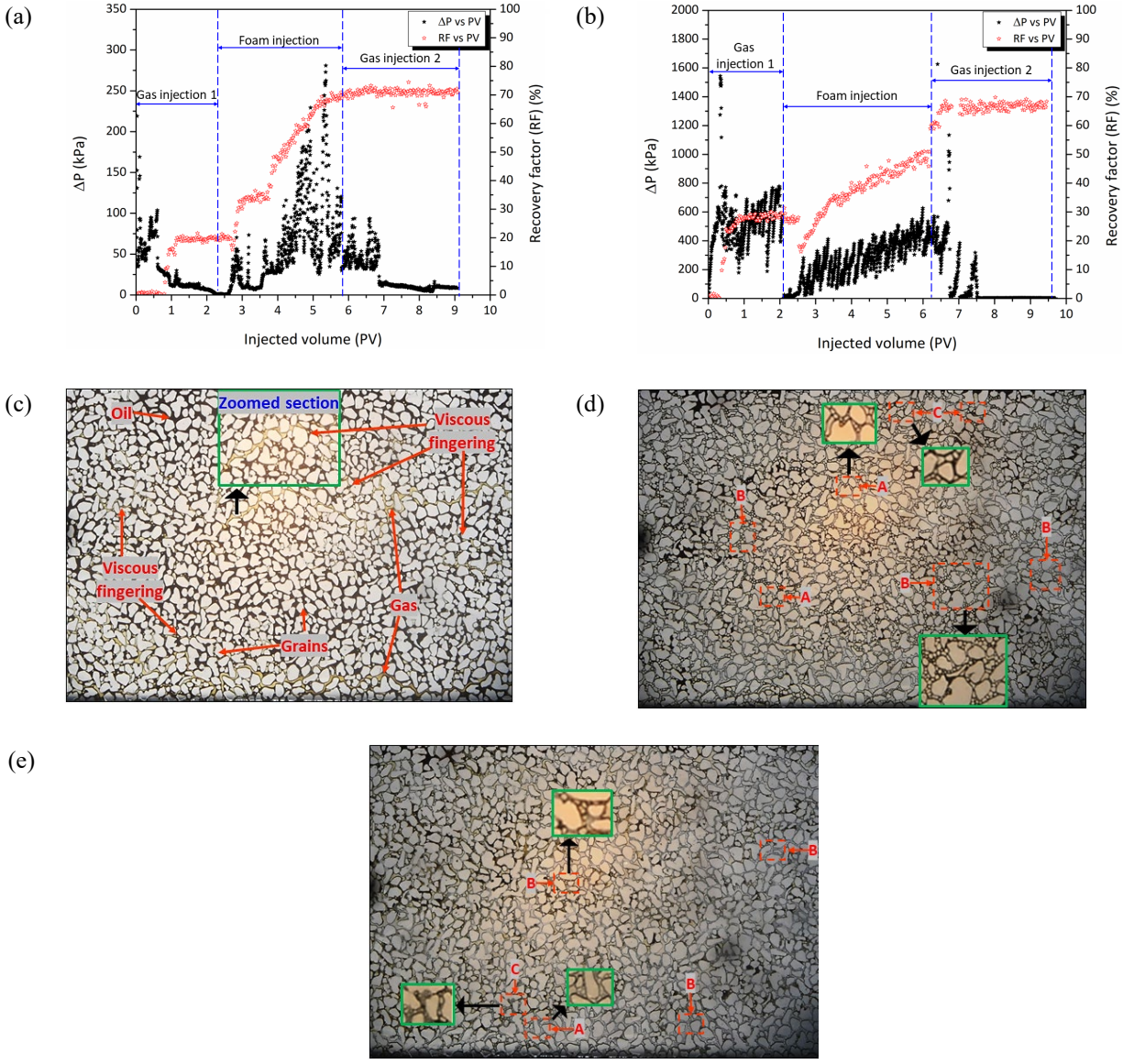

Fig. 2. Variation of oil recovery and ΔP with the injected volume of nitrogen gas followed by foam generated utilizing (a) alpha-olefin sulfonate and (b) customized-nanoparticle–surfactant solutions, (c) nitrogen gas flooding within a single permeability micromodel illustrating displacement of oil by injected gas and viscous fingering of gas through the oil, principal mechanisms of foam generation [A: snap-off, B: Lamella division, and C: leave behind] for (d) alpha-olefin sulfonate and (e) customized-nanoparticle–surfactant solutions.

Furthermore, Figure 3 shows the incidences of oil emulsification during the foam flow within a single permeability micromodel. During foam flow through porous media, emulsification typically induces the coalescence of previously disconnected oil ganglia. This aggregation results in enlarged oil clusters located at the leading edge of the advancing foam front. This results in accumulations of oil, which is subsequently mobilized towards the production outlet within the micromodel. Contrary to this, oil emulsification can also harm foam by causing oil to spread throughout the foam's lamella and Plateau border. This weakens the foam by forming oil bridges that lead to the detachment of foam lamella and ultimately causes the foam to collapse [26]. The aforementioned phenomenon was notably observed in case of alpha-olefin sulfonate-generated foam, manifesting as abnormal fluctuations in ΔP values (see Figure 2a). Alternatively, nanoparticles exhibit a capacity to mitigate structural damage within foam, thereby enhancing both stability and performance. Moreover, a reduction in fluctuations in ΔP values was observed (see Figure 2b).

The increase in total oil recovery and variation in ΔP values from gas and foam floodings in a dual permeability micromodel are shown in Figure 4 (a, b). Moreover, the average total oil recovery summary at the end of each

flooding is shown in Figure 4 (c, d) and Table 2. The dominant viscous fingering and channeling of gas within the K_L zone relative to the K_H zone are shown in Figure 5a. Within K_L zones, distinct pathways of injected nitrogen gas are evident, resulting in substantial regions of unrecovered oil. Conversely, within K_H zones, nitrogen gas exhibited less channeling and fingering, attributed to the more uniform distribution of pore networks. This results in a more efficient oil displacement and, hence, more oil recovery. Moreover, in K_H zone, a favorable mobility ratio between the oil and injected gas can be achieved. Contrary in K_L zone, injected gas could not penetrate oil effectively. This occurs because the gas flows quickly to the K_H zone, leaving the oil behind in the K_L zone due to differences in permeability. As a result, there is reduced oil recovery due to inefficient oil displacement.

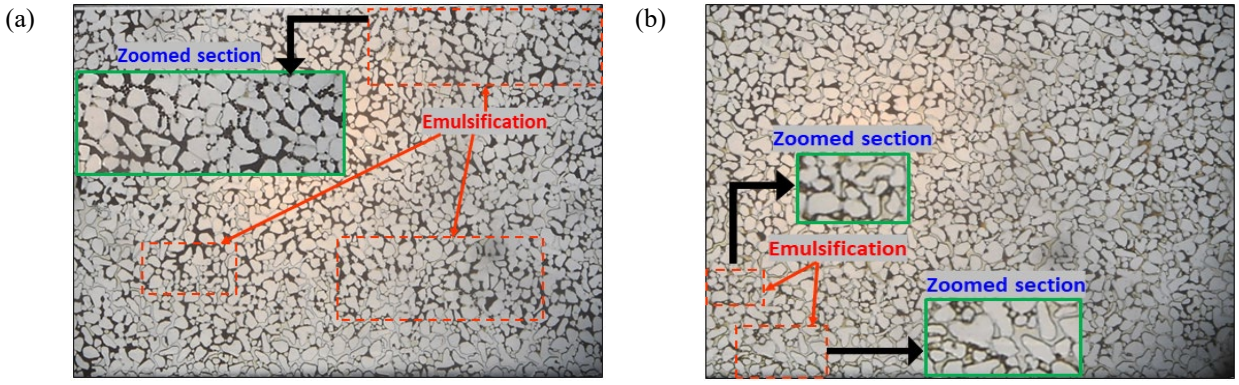

Fig. 3. Emulsification of oil by (a) alpha-olefin sulfonate-generated foam and (b) customized-nanoparticle–surfactant-generated foam.

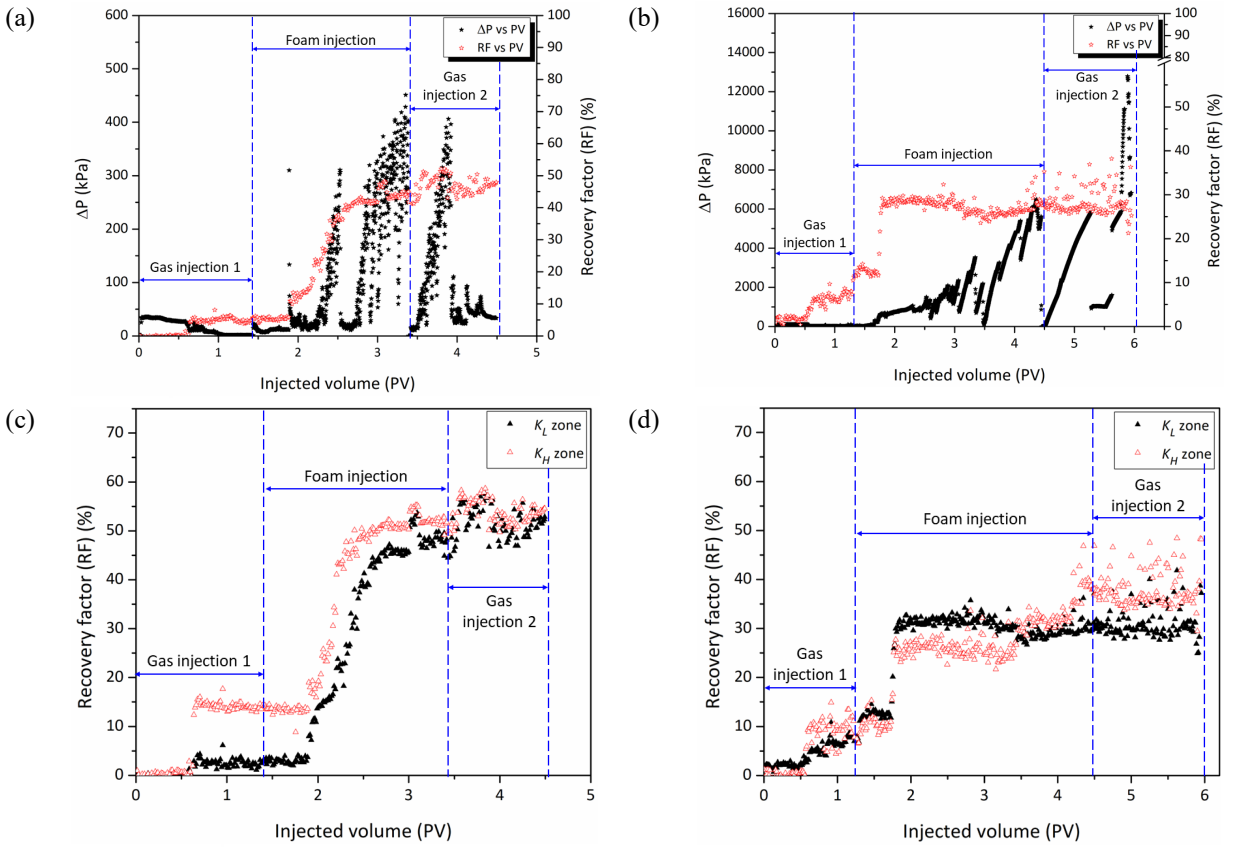

Fig. 4. Variation of oil recovery and ΔP by the injected volume of nitrogen gas with foam generated utilizing (a) alpha-olefin sulfonate and (b) customized-nanoparticle–surfactant solutions in dual permeability micromodel, oil recovery from the K_L and K_H zones in relation to the amount of nitrogen gas injected, followed by (c) alpha-olefin sulfonate-generated foam and (d) customized-nanoparticle–surfactant-generated foam.

Table 2. Oil recovery achieved using gas and foam injections.

Composition	Single permeability			Dual permeability								
	Gas flooding 1	Foam flooding	Gas flooding 2	Gas flooding 1 recovery			Foam flooding recovery			Gas flooding 2 recovery		
				K_L	K_H	Total ROI	K_L	K_H	Total ROI	K_L	K_H	Total ROI
Alpha-olefin sulfonate	20.2	49.2	2.0	3.1	14.1	5.1	45.6	37.8	39.1	2.1	1.6	3.4
Customized-nanoparticle–surfactant	28.7	37.7	0.4	7.9	10.3	7.3	22.0	26.6	20.4	0.7	3.7	0.2

Even though the alpha-olefin sulfonate-generated foam has more significant total ROI than customized-nanoparticle–surfactant-generated foam, it is clear from Figure 5 (b, c) that customized-nanoparticle–surfactant-generated foam performed better in the K_L zone than alpha-olefin sulfonate-generated foam. This is due to the clear visuals of dominant oil emulsification in both the K_L and K_H zones of the micromodel. As previously discussed, oil emulsification could adversely impact foam stability. Specifically, emulsified oil can disperse throughout the foam structure's lamella and Plateau borders, weakening the foam. This weakening occurs through the formation of oil bridges, which lead to the detachment of foam lamellae and ultimately result in foam collapse. Additionally, this phenomenon could contribute to the significant variations in ΔP observed in the case of foams generated with alpha-olefin sulfonate injection (see Figure 4a). Contrary, the addition of nanoparticles helps to strengthen the foam structure, reducing coalescence and drainage of the liquid phase, thus improving foam stability in the porous media [17]. Furthermore, a notable stability in ΔP values (see Figure 5b), and reduction in premature gas channeling and fingering occurrences are observed when comparing customized-nanoparticle–surfactant-generated foam to alpha-olefin sulfonate-generated foam (see Figure 5 (b, c)).

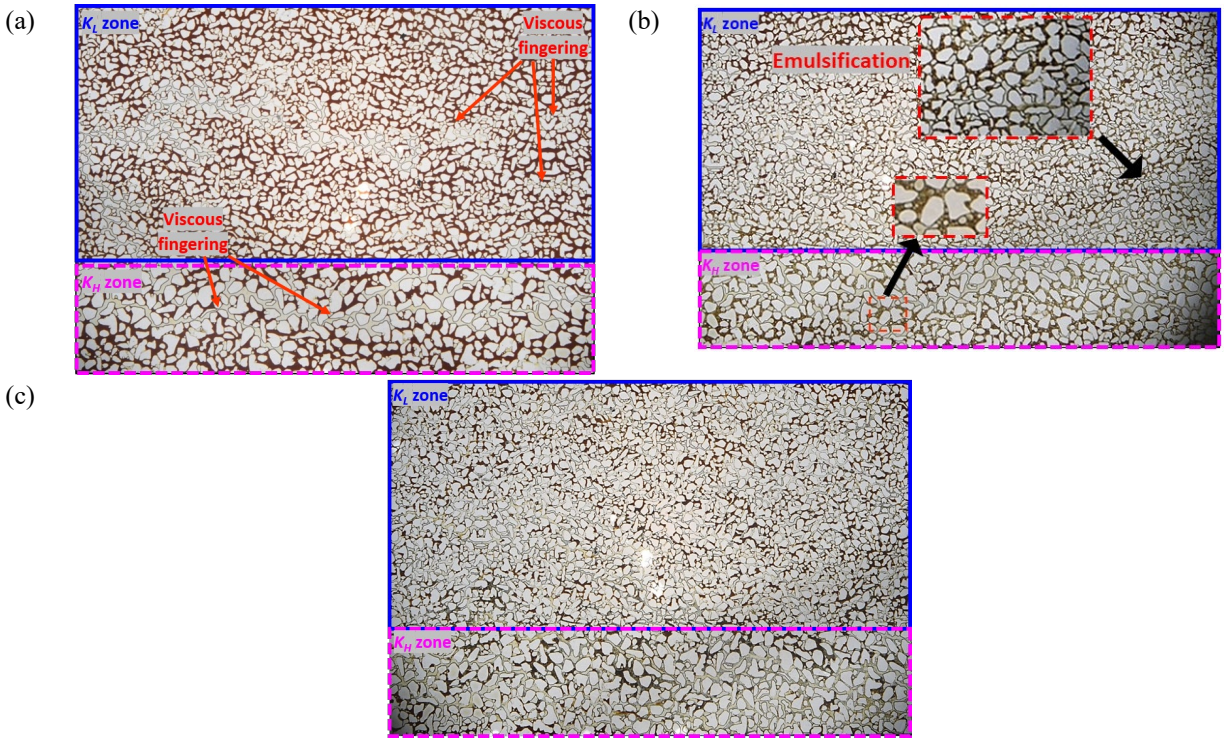

Fig. 5. (a) Nitrogen gas flooding within a dual permeability micromodel illustrating displacement of oil by injected gas and viscous fingering of gas through the oil, propagation of (b) alpha-olefin sulfonate and (c) customized-nanoparticle–surfactant foams in dual permeability micromodel.

4 Conclusions and recommendations for future work

The present investigation examines the effectiveness of customized-nanoparticle–surfactant-generated foam for oil recovery application, further compared with foam generated via a commercial alpha-olefin sulfonate surfactant solution by utilizing single and dual permeability micromodels. An increase of 13.7–26.6% oil recovery was observed through customized-nanoparticle–surfactant-generated foam injection in the micromodel. Nevertheless, in cases of core flooding examinations, these values can differ. Although alpha-olefin sulfonate-generated foam exhibited a higher oil recovery efficiency than customized-nanoparticle–surfactant-generated foam, it displayed instability including noteworthy fluctuations in ΔP and visualizations of gas breakthroughs. Conversely, the customized-nanoparticle–surfactant-generated foam demonstrated greater stability. Additionally, fluctuations in ΔP were limited. Furthermore, the robust foam generated using customized-nanoparticle–surfactant solutions effectively obstructed high permeability zones, redirecting flow towards low permeability zones, thereby improving the oil recovery.

This study did not examine key foam parameters such as foam quality and apparent viscosity, which are crucial for comprehending foam behavior in porous media. Instead, the research concentrated on observing foam movement and oil displacement in porous media using direct visualization techniques under high pressure. Based on the insights gained from this study, we intend to undertake more detailed research into the influence of various interfacial properties, including the adsorption of chemical additives at oil–water interfaces and onto rock surfaces, on foam stability. Additionally, future investigations will focus on optimizing foam parameters such as foam quality, mobility reduction factor (MRF), and apparent viscosity under high pressure and temperature conditions, as these parameters are critical for the efficacy of foam-assisted EOR.

5 References

1 J. Machale, S. K. Majumder, P. Ghosh, and T. K. Sen, Rev. Chem. Eng. **36**, 789–830 (2020).

2 J. Sheng, *Modern chemical enhanced oil recovery: Theory and practice*. (Gulf Professional Publishing, Massachusetts, USA, 2010).

3 L. C. Burrows, F. Haeri, P. Cvetic, S. Sanguinito, F. Shi, D. Tapriyal, A. Goodman, and R. M. Enick, Energy Fuels **34**, 5331–5380 (2020).

4 C. Negin, S. Ali, and Q. Xie, Petroleum **2**, 324–333 (2016).

5 A. A. Olajire, Energy **77**, 963–982 (2014).

6 J. J. Taber, F. Martin, and R. Seright, SPE Reservoir Eng. **12** (3), 189–198 (1997).

7 J. Machale, S. K. Majumder, P. Ghosh, T. K. Sen, and A. Saeedi, Chem. Eng. Commun. **209**, 143–157 (2022).

8 O. Massarweh and A. S. Abushaikha, Energy Rep. **6**, 3150–3178 (2020).

9 S. A. Farzaneh and M. Sohrabi, presented at the EAGE Annual Conference and Exhibition Incorporating SPE Europec, London, UK, 2013.

10 M. T. Janssen, A. S. Mutawa, R. M. Pilus, and P. L. Zitha, Energy Fuels **33**, 4951–4963 (2019).

11 J. J. Sheng, in *Enhanced Oil Recovery Field Case Studies* (Elsevier, Massachusetts, USA, 2013), pp. 251–280.

12 P. Ghosh, *Colloid and interface science*. (PHI Learning, New Delhi, India, 2009).

13 R. Pugh, Adv. Colloid Interface Sci. **64**, 67–142 (1996).

14 K. Z. Abdelgawad, A. R. Adebayo, A. Isah, and N. S. Muhammed, J. Pet. Sci. Eng. **211**, 110195 (2022).

15 M. Sagir, M. Mushtaq, M. Tahir, M. Tahir, and A. Shaik, in *Surfactants for Enhanced Oil Recovery Applications* (Springer, Cham, Switzerland, 2020), pp. 41–63.

16 H. Hematpur, S. M. Mahmood, N. H. Nasr, and K. A. Elraies, J. Nat. Gas Sci. Eng. **53**, 163–180 (2018).

17 M. Issakhov, M. Shakeel, P. Pourafshary, S. Aidarova, and A. Sharipova, Pet. Res. **7**, 186–203 (2022).

18 Q. P. Nguyen, A. V. Alexandrov, P. L. Zitha, and P. K. Currie, presented at the SPE International Conference and Exhibition on Formation Damage Control, Lafayette, Louisiana, USA, 2000.

19 N. Yekeen, M. A. Manan, A. K. Idris, E. Padmanabhan, R. Junin, A. M. Samin, A. O. Gbadamosi, and I. Oguamah, J. Pet. Sci. Eng. **164**, 43–74 (2018).

20 J. Machale, D. A. Akrong, O. Mohammadzadeh, A. Telmadarreie, A. Yethiraj, and L. A. James, presented at the The 36th International Symposium of the Society of Core Analysts, Abu Dhabi, UAE, 2023.

21 K. Ahmadi, D. A. Akrong, E. A. Sripal, F. Sahari Moghaddam, E. K. Ovwigho, C. Esene, J. Machale, A. Telmadarreie, and L. A. James, presented at the Offshore Technology Conference, Houston, Texas, USA, 2023.

22 M. Mahmoodi, L. James, and T. Johansen, J. Pet. Sci. Eng. **167**, 829–843 (2018).

23 A. Telmadarreie and J. J. Trivedi, Transport Porous Media **113**, 717−733 (2016).

24 M. Sahimi, M. Reza Rasaei, and M. Haghighi, in *Gas Transport in Porous Media* (Springer, 2006), pp. 133−168.

25 M. Shafiei, Y. Kazemzadeh, M. Escrochi, F. B. Cortés, C. A. Franco, and M. Riazi, Sci. Rep. **14**, 7468 (2024).

26 N. Yekeen, M. A. Manan, A. K. Idris, A. M. Samin, and A. R. Risal, J. Dispersion Sci. Technol. **39**, 623−633 (2018).

27 R. Singh and K. K. Mohanty, Energy Fuels **29**, 467–479 (2015).

28 H. Wang, Y. Gong, W. Lu, and B. Chen, Appl. Surf. Sci. **254**, 3380−3384 (2008).

29 G. Yu and W. Rossen, J. Pet. Sci. Eng. **214**, 110406 (2022).